Epidemiological Dynamics of SARS-CoV-2 in White-tailed Deer

Joshua Hewitt (joshua.hewitt2@usda.gov)
United States Department of Agriculture https://orcid.org/0000-0002-0844-7769
Grete Wilson-Henjum
United States Department of Agriculture
Derek Collins
United States Department of Agriculture
Timothy Linder
U.S. Department of Agriculture https://orcid.org/0000-0003-3440-0574
Julianna Lenoch
U.S. Department of Agriculture
Jonathon Heale
United States Department of Agriculture
Christopher Quintanal
United States Department of Agriculture
Robert Pleszewski
United States Department of Agriculture
Dillon McBride
The Ohio State University
Andrew Bowman
The Ohio State University https://orcid.org/0000-0002-0738-8453
Jeffrey Chandler
U.S. Department of Agriculture
Susan Shriner
United States Department of Agriculture https://orcid.org/0000-0003-0349-7182
Sarah Bevins
U.S. Department of Agriculture
Dennis Kohler
USDA APHIS Wildlife Services National Wildlife Disease Program
Richard Chipman
United States Department of Agriculture
Allen Gosser
United States Department of Agriculture
David Bergman

United States Department of Agriculture

Thomas DeLiberto

U.S. Department of Agriculture https://orcid.org/0000-0003-1115-1472

Kim Pepin

U.S. DEPARTMENT OF AGRICULTURE

Article

Keywords:

Posted Date: April 21st, 2023

DOI: https://doi.org/10.21203/rs.3.rs-2842780/v1

Additional Declarations: There is **NO** Competing Interest.

Epidemiological Dynamics of SARS-CoV-2 in White-tailed Deer

Joshua Hewitt[1*], Grete Wilson-Henjum[1], Derek T. Collins[2], Timothy J. Linder[2], Julianna B. Lenoch[2], Jonathon D. Heale[3], Christopher A. Quintanal[4], Robert Pleszewski[4], Dillon S. McBride[5], Andrew S. Bowman[5], Jeffrey C. Chandler[4], Susan A. Shriner[1], Sarah N. Bevins[2], Dennis J. Kohler[2], Richard B. Chipman[3], Allen L. Gosser[3], David L. Bergman[3], Thomas J. DeLiberto[3], Kim M. Pepin[1]

[1]National Wildlife Research Center, Wildlife Services, Animal and Plant Health Inspection Service, United States Department of Agriculture, Fort Collins, CO, USA
[2]National Wildlife Disease Program, Wildlife Services, Animal and Plant Health Inspection Service, United States Department of Agriculture, Fort Collins, CO, USA
[3]Wildlife Services, Animal and Plant Health Inspection Service, United States Department of Agriculture, Fort Collins, CO, USA
[4]Wildlife Disease Diagnostic Laboratory, Wildlife Services, Animal and Plant Health Inspection Service, United States Department of Agriculture, Fort Collins, CO, USA
[5]Veterinary Preventive Medicine, The Ohio State University College of Veterinary Medicine, Columbus, OH, USA
[*]Corresponding author: joshua.hewitt2@usda.gov

Abstract

Understanding pathogen emergence in new host species is fundamental for developing prevention and response plans for human and animal health. We leveraged a large-scale surveillance dataset coordinated by United States Department of Agriculture, Animal and Plant Health Inspection Service and state natural resources agencies to quantify infection of SARS-CoV-2 in North American white-tailed deer (*Odocoileus virginianus*; WTD) using a hierarchical epidemiological model in the eastern half of the United States. Our model found that male deer had higher positivity than female deer, and positivity was higher in counties with higher human population density or deer habitat. Estimated SARS-CoV-2 local epidemiological reproduction numbers were between 1 and 2.5 in most well-sampled counties, with local epidemics in WTD peaking earlier in the northeast and mid-Atlantic relative to the Midwest and Southeast. Similar peak infection prevalence times across many counties provided indirect evidence for widespread transmission via human-to-deer spillover, while the widespread high estimates of local epidemiological reproduction number suggested that sustained deer-to-deer transmission is also probable. The model estimated 10% of infected WTD were infected due to human infection pressure.

1 Introduction

Starting in 2020, SARS-CoV-2 was found in white-tailed deer [WTD; 1, 2]. By 2021, there was evidence of regional transmission in WTD through a combination of ongoing deer-to-deer and human-to-deer transmission [2–5]. Endemic transmission of SARS-CoV-2 in WTD could position these populations as reservoir hosts, posing risk for variant persistence [4, 6], evolution of new variants [7, 8], and spillback into human populations [7–9]. Cross-species transmission can have global health impacts during a pandemic. For example, pandemic H1N1 Influenza virus (H1N1pdm09) was introduced into humans from animals [10], resulting in ongoing animal-human transmission and viral evolution globally [11–13]. These patterns highlight the need to better understand drivers of zoonotic pathogens establishing and persisting in new species to inform science-based One Health decisions, improve risk assessment, and plan effective surveillance, early response, and mitigation strategies.

Chandler et al. [1] initially documented the presence of virus neutralizing antibodies to SARS-CoV-2 in free-ranging WTD. Experimental infection studies demonstrated the susceptibility of WTD to SARS-CoV-2 infection, shedding of live virus primarily through oral/nasal secretions, deer-to deer transmission, and the persistence of neutralizing antibodies for up to several weeks following infection [14, 15]. A later study revealed that WTD can maintain antibodies for at least 13 months [16]. Deer-to-deer transmission may

occur within wild populations beyond the initial introduction period. Surveillance studies in WTD have shown persistence of SARS-CoV-2 alpha and gamma variants in populations 4-6 months after their peak circulation and extinction in the human population [4, 5, 17, 18]. These data describing susceptibility and transmission capabilities of SARS-CoV-2 in WTD and the fact that WTD are abundant and share a variety of habitats with humans across the United States [19], highlight the need to understand potential infection dynamics of SARS-CoV-2 in WTD across the range of the species.

Until recently, SARS-CoV-2 surveillance in WTD has only been conducted and described at the scale of a single state, province, or region [1, 2, 4, 7], with sampling occurring during a 3 to 4-month window. This made it challenging to understand how widespread SARS-CoV-2 is in WTD, its epidemiological dynamics, and associated ecological drivers. Recently, the United States Department of Agriculture (USDA) has been working with state wildlife agencies in conducting widespread surveillance of SARS-CoV-2 in WTD to address these gaps [5, 17]. Here, we use data from a surveillance program of SARS-CoV-2 in WTD [17] to estimate the spatial distribution of true prevalence, infection rates and their relationship to specific risk factors, and the temporal dynamics of initial invasion into WTD across their range over 13 months.

The national-scale surveillance data are collected by opportunistically sampling hunter-harvested deer and through targeted agency management. Different sub-populations are sampled unequally in space, time, and overall numbers (e.g., female vs. male WTD, or WTD in suburban/urban or rural human populations). Sample composition tends to be more challenging to account for using (descriptive) statistics, confidence intervals, and hypothesis tests designed for other sampling designs such as non-stratified, simple random sampling [20]. To address the challenges of inference from opportunistic sampling, we developed a hierarchical model that accounts for sample composition in estimates of population-level parameters and predictions. Our model used spatially and temporally correlated susceptible-infected-recovered (SIR) curves, commonly used for epidemiological inference [21–28], to account for trends across time, space, sample composition, and potential transmission from humans to deer. Our model also used county-level data as covariates to estimate the influence of deer habitat and human presence and infection on WTD infection risk. In particular, we use the model to estimate the overall proportion of WTD infected due to human infection pressure (i.e., spillover). Model based methods to analyze disease surveillance data can extend the utility of surveillance data, for example, by allowing disease prevalence to be estimated in counties and at times when direct surveillance through sampling is not possible.

2 Results

2.1 Description of sample composition and descriptive statistics

From October 2021 through March 2022 there were 10,217 nasal or oral swab samples from WTD tested from 27 states and Washington, DC. SARS-CoV-2 viral RNA was detected in 13% (1,307) of the 10,217 samples [17, 18]. The raw, apparent prevalence summaries are descriptive statistics that do not account for the opportunistic sample collection. There were similar numbers of samples collected from both sexes (males = 5,076, females = 5,141), but SARS-CoV-2 viral RNA was detected more often in males (15%) relative to females (11%). Adults (8,000 samples) were more heavily sampled than juveniles (2,217 samples), but detection rates were similar in both groups (13% vs. 12%). Nasal swabs (9,343 samples) were collected more often than oral swabs (364 samples), and 510 samples had missing data describing swab type. Infection rates (i.e., proportion positive) appeared higher in oral and unknown swabs (16% and 17%, respectively) relative to nasal swabs (12%). For management method, hunter-harvest samples were most common (4,577 samples with 17% positive), followed by samples collected from USDA removal and management purposes (agency management; 3,866 samples with 11% positive) or other mortalities (e.g., roadkill; 1,774 samples with 6% positive). Hunter harvest samples were collected during a shorter time window (i.e., hunting seasons), while agency management and other mortalities were collected more consistently throughout the full period of surveillance.

2.2 Risk factors

2.2.1 The model captures the data well

We inferred the effects of ecological risk factors using a hierarchical model of the surveillance data that included a sample-level component for inferring individual infection risks p_k while estimating population-level SARS-CoV-2 local epidemiological reproduction numbers R_ℓ from the SIR component of the model. A calibration curve showed that p_k predicted positive and negative test outcomes well (Figure 1), and that estimates of p_k are close to apparent prevalence (observed data) with underprediction in regions with high predicted prevalence. The model fit builds confidence that the method can estimate prevalence in counties and at times when direct surveillance through sampling was not possible due to limited resources. The model fit also builds confidence that the method can also estimate epidemiological characteristics of SARS-CoV-2 in WTD, such as peak prevalence and outbreak timing across counties.

2.2.2 Sex and management method are the only significant sample-level variables

For sample-level factors, we found a significant interaction of sex and management method, but no significant effect between oral and nasal swab types or age class (Table 1). Male deer samples collected by agency management tended to have higher infection than female deer (Row a_2 in Table 1, Figure 2; 14% positive males, 10% positive females from October 2021 through March 2022), but the effect was less pronounced for male deer harvested by hunters (Row a_10 in Table 1, Figure 2; 10% positive males, 8% positive females from October 2021 through March 2022).

2.2.3 Effects of inhabitable deer area are weaker than effects of human population density

For county-level effects, there is some evidence for weak relationships between local epidemiological reproduction rate R_ℓ and covariates. The effects of deer habitat (a proxy for deer abundance) and human population density are positive but marginally not significant (Rows b_2 and b_3 in Table 1, Figure 3). Predicted prevalence in WTD increased from 10% when human population density was 10 people per sq. km. to 15% when human population density was 100 people per sq. km. from October 2021 through March 2022 (Figure 3). Predicted prevalence in WTD also increased from 10% when the proportion of WTD habitat is low (i.e., near 0) to 15% when WTD habitat is high (i.e., near 1) from October 2021 through March 2022. (Figure 3). However, there was a substantial amount of variation in the relationships between prevalence in WTD and human population density or proportion of WTD habitat. Deer habitat is estimated via the Gap Analysis Project (GAP) species distribution model [29]. Here, we quantify deer habitat as the GAP-estimated proportion of a county's land area that is inhabitable to WTD.

2.2.4 Role of human SARS-CoV-2 infection on WTD SARS-CoV-2 infection

The model estimates that SARS-CoV-2 prevalence in WTD tends to increase with SARS-CoV-2 infection in humans. The model uses the human SARS-CoV-2 death rate as a lagged, proxy-indicator for infection. The model estimates the odds of WTD prevalence increases by 13% for every additional 11 human deaths per 100,000 county residents (logistic regression parameter interpretation for row a_8 in Table 1; 95% highest posterior density interval (HPDI) spans from 1% decrease to 31% increase). The model also estimates that, on average, 10% of positive deer detected were due to human infection pressure from October 2021 through March 2022 (95% HPDI: 0–16%).

2.2.5 Local epidemiological reproduction numbers greater than 1 are widespread

Estimates of the local epidemiological reproduction number R_ℓ were greater than 1 in nearly all counties in states where samples were collected and ranged up to 2.5 in some counties (Figure 4A). However, there is also large uncertainty in R_ℓ estimates in states where few samples were collected such that R_ℓ could have been less than 1 for many Mid- and South-western counties (Figure 4).

2.2.6 Estimates of time-averaged prevalence was at least 3% in most sampled counties

Estimates of average prevalence from October 2021 through March 2022 tended to be higher on the East coast than in the Mid- and South-West (i.e., time-averaged prevalence; Figure 5A). The model-based estimates adjust for varying sample collection rates over time. The average county-level apparent prevalence (Figure 5B; the proportion of positive test results per county) was more extreme (i.e., higher or lower) than time-averaged estimates in counties with low sample sizes (Figure 5D). Importantly, uncertainty in time-averaged prevalence estimates (Figure 5C) was also higher in counties with low sample sizes. Predicted peak prevalence varied spatially across the range of WTD studied.

2.2.7 Peak prevalence occurred earliest in counties in the northeast and mid-Atlantic

Peak prevalence occurred later in counties in the Midwest and Southeast (Figure 6A). However, there was local variation across counties within a state. In New York, peak prevalence is predicted to have occurred 1–3 months earlier in the western counties compared to the eastern counties (Figure 6A). However, uncertainty in predicted timing is higher in the eastern counties of New York compared to the western counties (Figure 6B). Examination of SARS-CoV-2 prevalence in WTD over time predicted outbreak start, peak prevalence, and prevalence decline occurred earlier in Onondaga County, New York than in Cuyahoga County, Ohio; the two most intensively sampled counties in our study (Figure 7). Comparison to human death rate data illustrates how SARS-CoV-2 in humans is not necessarily a primary driver for SARS-CoV-2 prevalence in WTD, but can prolong the duration of an outbreak in WTD.

3 Discussion

Large-scale surveillance data provided evidence for substantial deer-to-deer transmission in addition to widespread spillover from human-to-deer populations [5]. High estimates for the SARS-CoV-2 local epidemiological reproduction number R_ℓ (i.e., up to 2.5) suggested that sustained deer-to-deer transmission was probable following disease introduction to local deer populations (Figure 4). Model estimates suggested

SARS-CoV-2 in WTD was present in most counties that can support WTD populations (i.e., WTD habitat) across the Conterminous United States (CONUS; Figure 5). Estimates for the time at which peak infection prevalence occurred are similar for many counties sampled, which provided indirect evidence for widespread transmission via human-to-deer spillover (Figure 6). By comparison, in the absence of spillover, disease transmission across space should primarily be driven by diffusion between neighboring counties, which would yield a smoother spatial pattern in disease timing [30]. Data indicates that differences between peak infection in humans and WTD can differ as well (Figure 7). Different timing for disease in humans and WTD might suggest concurrent widespread deer-to-deer transmission in addition to human-to-deer spillover.

The number and rate of disease transmission events from humans to deer are difficult to estimate. Phylogenetic studies of surveillance data estimate the number and timing of spillover events within the dataset [2–5, 18]. However, the number and rate of disease transmission events from humans to deer can be difficult to estimate at a national population level because of challenges with sampling designs (i.e., both human and deer sampling designs are biased and deer abundances are unknown). While SIR models do not identify individual spillover events, the human infection proxy within the sample-level model equation (1) can be used to estimate feasible ranges for the relative frequency of deer-to-deer vs. human-to-deer transmission events. The modeling framework statistically attributes "excess infection" relative to the SIR model's baseline infection process equation (2) as potential spillover pressure.

Posterior summaries for the risk factors identified in Table 1 suggest potential implications for general knowledge of SARS-CoV-2 in WTD and ongoing surveillance programs. The model suggested that male deer were infected at higher rates than female deer. Similar sex-related differences occur for chronic wasting disease (CWD), bovine tuberculosis, and other infectious diseases [31–33]. Sex-related differences are often explained by hypotheses that male deer have different social behavior, larger home range sizes, and breeding season movements, leading to wider and more frequent contact with other groups of deer than females [33].

Although descriptive summaries of the raw data suggested that prevalence differed for management method (i.e., Hunter vs. Agency) and swab type (i.e., Oral vs. Nasal), the model did not find strong evidence for this pattern once the imbalanced sampling design factors were accounted for together, suggesting that surveillance data collected from these different sources and methods can be analyzed together.

Local epidemiological reproductive rate of SARS-CoV-2 in WTD appeared to weakly increase with human population density. This might suggest that areas with higher human density have greater opportunity for reverse zoonotic transmission, contributing to the force of infection in deer. The effect of human density was relatively small with ample variation. Our model did not consider changes to human density across time, which likely does not accurately reflect human movement and contact patterns with deer because we did not have such data. For instance, the effect of areas such as campgrounds that see pulses of human

density at irregular time intervals (i.e., around holidays) would not be captured by static human densities. Furthermore, natural areas such as parks and campgrounds that have pulses of human activity are also places where humans are likely to encounter a deer. Finer scale data on human mobility and human-deer contact frequencies in different settings would improve our understanding of this relationship and enable identification of additional landscape variables that could help identify how spillover is occurring and be included in risk mapping.

Disease transmission pressure from humans to deer is also difficult to quantify because disease surveillance in humans is challenging. Surveillance of SARS-CoV-2 in humans requires extensive funding and consistent community participation. Surveillance is further challenging because positive at-home tests are generally not included in official reporting. The human death rate served as a proxy for human infection during early stages of the pandemic. However, the proxy becomes increasingly uninformative as effective treatments become available and survival increases. Future evaluation of SARS-CoV-2 in WTD may require different proxies for human infection.

The model further suggested that SARS-CoV-2 local epidemiological reproductive rate increased with the proportion of a county's land that supports WTD populations, albeit weakly. In lieu of using WTD density estimates, we used the proportion of a county's land that WTD can inhabit (i.e., WTD habitat) to approximate where WTD might be more densely populated. We chose this approach because WTD density information is limited to small-scale studies due to the difficulty of collecting this data [34], and methods for state-level abundance estimation vary across states, which introduces additional variation. Increased habitat suitability is tied to increased incidences of CWD in WTD [35], with the supporting hypothesis that suitable habitat supports higher density of WTD. The effect seen here might suggest infection reproduction is facilitated through deer-to-deer contact. However, finer scale WTD density information or habitat data that more closely informs WTD density would provide further insight to this relationship.

Quantifying disease dynamics requires intensive data distributed throughout time and space. In this study, we used an opportunistic sampling design, which incurred temporal and spatial data gaps. These data gaps propagated uncertainty in our estimates of SARS-CoV-2 prevalence in WTD (Figure 5C). Uncertainty in these estimates could be reduced through continued sampling in counties where long-term sampling has already taken place. Furthermore, new sampling in counties that do not currently have data and are distant from well-sampled counties (e.g., represent different values in of covariates such as proportion of land inhabitable to WTD, human density, human case rates, or other potential risk factors that have yet to be explored) would bolster the confidence of these estimates. However, requirements for reducing estimate uncertainty can change over time, and would be best addressed using an adaptive sampling design. Another limitation of this study is the spatial resolution at which disease dynamics could be described (i.e.,

county level). Our description of national SARS-CoV-2 dynamics in WTD would be augmented through the implementation of intensive sampling within specific populations with location data where samples are collected (i.e., a more appropriate scale understanding transmission dynamics and their risk factors). Another key gap is to include repeated long-term sampling at specific locations spread across different ecosystems. This will help to disentangle the drivers of infection dynamics and persistence both within and across populations - the subject of our ongoing work.

Accurate quantification of disease dynamics and their corresponding risk factors provides a platform for identifying optimal strategies for risk-based surveillance, prevention, early response, and control of zoonotic diseases. Surveillance programs can only partially observe disease trajectories due to limited resources. Model-based analyses of surveillance data can use estimates of disease prevalence at all points in space and time to fill in data collection gaps. Prevalence estimates can be interpreted as reconstructions of disease trajectories. Spatially analyzing reconstructed disease trajectories can identify regions that have been heavily impacted by disease and are potentially at increased risk for future outbreaks.

4 Methods

4.1 Data

4.1.1 Surveillance of SARS-CoV-2 in white-tailed deer

We present a detailed epidemiological analysis of data collected from surveillance studies described in Bevins et al. [17] and McBride et al. [18]. From October 2021 to September 2022 there were 10,722 WTD samples collected from 27 states and Washington, DC (Figure 5D). WTD samples were collected postmortem from multiple sources, including hunter harvest samples collected by state departments of natural resources, management events conducted by USDA Animal and Plant Health Inspection Service (USDA-APHIS), Wildlife Services [described in 17], and opportunistic sampling of mortalities such as roadkill collected by all agencies. Management type and individual deer-specific metrics including sex and age class were recorded. Removal location data was collected at the county level. When available, hunters were asked to disclose the county of removal, but in lieu of removal county, the check station county where the sample was collected was used. Nasal or oral swabs were collected and tested for the presence of SARS-CoV-2 viral RNA via rRT-PCR as previously described [17, 18].

4.1.2 County-level covariates

We estimated human density for each county using 2020 Census Bureau population data, which includes information about county area [36]. We divided the population of each county by the county area (km2). We calculated the proportion of each county's land that can support WTD populations (i.e., WTD habitat) using the Gap Analysis Project (GAP) WTD species distribution model [29]. The GAP WTD distribution model predicts species occurrence across GAP landcover classes based on empirical occupancy and habitat association analyses. GAP landcover class pixels are converted to a binary based on if that pixel represents suitable year-round WTD habitat. We used the total area covered by WTD habitat pixels within a county divided by the total county area to calculate the proportion of WTD habitat in each county.

4.1.3 County-level time-varying incidence and mortality rates for SARS-CoV-2 in humans

We calculated the weekly new death rate of SARS-CoV-2 in humans per county (cases per 100,000 people) using data from The New York Times repository of SARS-CoV-2 cases. Data are based on reports from state and local health agencies. The New York Times aggregates daily case and death counts published on state and local health department websites. We grouped each county's daily death report by week (Sunday-Saturday) and selected the first day of each week that data was reported. We then took the difference between the focal week's cumulative count and the cumulative count from two weeks prior to a deer sample's removal date to derive the case load in the two weeks prior to sampling. We divided the case load by the county population size [36] and multiplied this by 100,000 to derive death incidence per 100,000. The death rate serves as a lagged proxy for human SARS-CoV-2 infection that does not depend on human surveillance testing rates.

4.2 Statistical analyses

4.2.1 Spatially-varying SIR model

We specify a hierarchical Bayesian model that uses sample-level test results to estimate epidemiological parameters, associations with potential risk factors, and prevalence over time. Spatially and temporally correlated, county-level susceptible-infected-recovered (SIR) compartmental models account for trends across time and space. The model uses both sample- and county-level covariates to influence SIR model parameters, identifying potential risk factors for disease transmission. We apply the model to the 2,893 counties across CONUS estimated to support WTD populations and focus on the weeks over which samples were collected.

The model's response variable Y_k encodes the binary rRT-PCR test results for the kth sample such that $Y_k = 1$ for positive results and $Y_k = 0$ for negative results. The model treats Y_k as a Bernoulli random

variable with probability p_k of being positive. We interpret p_k as the individual infection risk or prevalence of SARS-CoV-2 for the kth animal's group, time, and location. The model uses the regression function specified via

$$\text{logit}\left(p_k\right) = \sum_j a_j z_{kj} + \text{logit}\left(i_{\ell_k}(t_k)\right) \tag{1}$$

to link rRT-PCR test results to county-level SIR curves and sample-level covariates and external conditions (e.g., age, sex, human death rate). The a_j and z_{kj} terms specify sample-level coefficients and covariates that adjust the baseline infected compartmet $i_{\ell_k}(\cdot)$ of the SIR curve for county ℓ_k at time t_k based on group-level characteristics and external conditions for sample k (see Table 1 for detailed covariate listing).

The SIR curve we propose models the proportion of susceptible $s_\ell(t)$, infected $i_\ell(t)$, and recovered $r_\ell(t)$ individuals in county ℓ at time t via spatially and temporally correlated systems of differential equations. The SIR system of differential equations for each county specified via

$$\begin{aligned} \frac{ds_\ell(t)}{dt} &= -\beta_\ell i_\ell(t) s_\ell(t), \\ \frac{di_\ell(t)}{dt} &= \beta_\ell i_\ell(t) s_\ell(t) - \gamma i_\ell(t), \\ \frac{dr_\ell(t)}{dt} &= \gamma i_\ell(t) \end{aligned} \tag{2}$$

uses a population-level recovery parameter γ and spatially varying deer-to-deer contact rate β_ℓ. Each county's SIR curve is modeled with a local outbreak time $t_{0,\ell}$ and common initial conditions $s_\ell(t_{0,\ell}) = s_0^*$, $i_\ell(t_{0,\ell}) = i_0^*$, and $r_\ell(t_{0,\ell}) = r_0^*$. Modeling SIR parameters and initial conditions with respect to spatial random effects and covariates accounts for spatial and temporal similarities in SIR curves between counties.

We model the county-level contact rate β_ℓ relative to the recovery rate γ scaled by a SARS-CoV-2 local epidemiological reproduction number R_ℓ for each county, such that $\beta_\ell = \gamma R_\ell$. The local epidemiological reproduction number quantifies the number of WTD to which a single infected WTD can be expected to transmit SARS-CoV-2 to naïve contacts. Covariates and spatially correlated random effects influence R_ℓ via

$$g(R_\ell) = \sum_j b_j x_{\ell j} + \eta_\ell, \tag{3}$$

to link R_ℓ to county-level covariates that can influence deer-to-deer contact rates (e.g., habitable area and human population density). The link function $g(\cdot)$ is an exponentially smoothed ramp that is linear for $0.1 < R_\ell < 10$ and decays to a low of $R_\ell = 0$ and a high of $R_\ell = 15$ (additional details in Supplement). The b_j and $x_{\ell j}$ terms specify county-level effects and covariates, and η_ℓ specifies a spatially correlated random

effect for each county (see Table 1 for detailed covariate listing). A conditional autoregressive (CAR) process model uses county adjacency reference information to model spatial connection and correlation for η_ℓ [37, Chapter 4]. The CAR model requires a spatial precision parameter τ_ℓ and a spatial range parameter γ_ℓ, both of which are estimated from data.

We also use a CAR process to model the local outbreak time $t_{0,\ell}$. Like η_ℓ, the CAR model for $t_{0,\ell}$ requires a spatial precision parameter τ_{t_0} and spatial range parameter γ_{t_0}. In conjunction with the other SIR curve parameters, the local outbreak time $t_{0,\ell}$ influences the time at which peak prevalence occurs.

All continuous covariates are scaled and shifted to have mean 0 and unit variance before model fitting. Standard prior distributions are assigned to unknown parameters (Supplement). Markov chain Monte Carlo (MCMC) methods are used to draw inference on model parameters and random effects. The model is run for 1,000,000 iterations, thinning to retain 10,000 samples to approximate the joint posterior distribution. Most of the spatial random effects for each county that support WTD populations across CONUS will not be precisely estimated because data is only collected from 589 of the 2,893 modeled counties. However, the model includes spatial random effects for all counties to inform spatial relationships between counties, and support risk mapping.

4.2.2 Spatio-temporal risk evaluation and mapping

The SIR model equation (2) can estimate spatially and temporally complete maps of SARS-CoV-2 prevalence for WTD after model fitting, filling in data collection gaps. Model fitting estimates SIR parameters for all counties ℓ and times t, so it is possible to estimate baseline prevalence $i_\ell(t)$ and other compartments at any point in time and space. Model fitting also estimates sample-level coefficients a_j, so it is also possible to replace the variables z_{kj}, ℓ_k, and t_k in equation (1) with appropriate substitutions z_{Gj}, ℓ, and t to estimate prevalence $p_{G\ell t}$ for an arbitrary demographic group and sample type G in county ℓ and time t. Within the Bayesian framework, composition sampling is the technical method that propagates uncertainty and dependence from estimates of parameters to estimates of prevalence, maps, and other features [37, p. 126]. The prevalence $p_{G\ell t}$ can be aggregated across both time and space, independently or together.

The time-averaged prevalence $p_{G\ell}$ for demographic group and sample type G in county ℓ is the average of the weekly prevalences $p_{G\ell 1}, p_{G\ell 2}, p_{G\ell 3}, \ldots$. Maps of $p_{G\ell}$ can illustrate where disease tended to be more widespread across the study period. Composition sampling, again, propagates uncertainty and dependence from estimates of parameters to estimates of $p_{G\ell}$.

The space-averaged prevalence p_{GAt} for demographic group and sample type G in area A summarizes all prevalence estimates $p_{G\ell t}$ for G at time t in area A. The summary p_{GAt} is a flexible weighted average

specified via

$$p_{GAt} = \sum_{\ell} w_{A\ell} p_{G\ell t}, \tag{4}$$

where $w_{A\ell}$ is the relative weight (or contribution) of county ℓ to area A at time t. For example, we can use equation (4) to estimate overall prevalence in state A at time t by setting $w_{A\ell} = 0$ for all counties outside state A. Within state A, we can set $w_{A\ell}$ proportional to the total area of state A's WTD habitat that falls within county ℓ. So, if 20% of state A's WTD habitat falls within county ℓ, then we set $w_{A\ell} = .2$. As with $p_{G\ell}$, composition sampling propagates uncertainty and dependence from estimates of parameters to estimates of p_{GAt}.

4.2.3 Spillover risk

We compare prevalence estimates that are both space and time-averaged to evaluate spillover. We use conditional probabilities to quantify spillover as the risk that, on average, an infected deer was infected due to human infection pressure. Using aggregation methods described in Section 4.2.2, the sample-level model equation (1) can estimate p_{DH} the time-averaged proportion of deer that were infected with SARS-CoV-2 across CONUS. The sample-level model can also estimate p_D the time-averaged proportion of deer that were infected with SARS-CoV-2 across CONUS in the absence of human infection pressure (i.e., through deer-to-deer transmission and other zoonoses). The estimate for p_D uses the fitted model to predict prevalence with all human SARS-CoV-2 data set to 0. The sample-level model is not designed to directly estimate the time-averaged proportion of deer infected due to human infection pressure p_H, but we assume the causes of infection are mutually exclusive, implying $p_{DH} = p_D + p_H$. The conditional probability $p_{H|DH} = 1 - p_D/p_{DH}$ exactly quantifies spillover as we defined it earlier. Composition sampling propagates uncertainty and dependence from estimates of parameters to estimates of $p_{H|DH}$.

Acknowledgements

Funding for this study was provided by the USDA American Rescue Plan. We thank the federal employees at USDA APHIS Wildlife Services, USDA APHIS National Wildlife Disease Program, and collaborators at state wildlife agencies for contributing wildlife sampling expertise, as well as hunters for participating in this large-scale effort. We would also like to acknowledge Joshua Eckery, and Jason Klemm from the USDA APHIS National Wildlife Research Center, for laboratory screening of swab samples. We are grateful for Kelsey Weir, Tim Linder, and Jourdan Ringenberg for their assistance in project development and implementation.

Sample collection in Ohio (DSM & ASB) was partially supported by the Centers of Excellence for Influenza Research and Response, National Institute of Allergy and Infectious Diseases, National Institutes of Health (NIH), Department of Health and Human Services, under contract 75N93021C00016.

Competing interests

The authors declare no competing interests.

Author contributions

All authors made substantial contributions to the writing and revision of the work. SS, JC, SB, TJD, JDH, AG, DB, TL, DC, JL, RC, CQ, RP, DM, and AB made substantial contributions to the acquisition and interpretation of data. RC, JL, DK, TJD, SS, AG, DB, SB, JC, DM, and AB made substantial contributions to development and implementation of the surveillance programs. JH, GW, and KP made substantial contributions to the conception of the analysis and interpretation of data. JH and GW made substantial contributions to the software used to implement the analysis.

Data availability and computer code

The complete dataset analysed in this study is not publicly available due to sensitive sample-level collection information, such as detailed sample collection locations and dates, but can potentially be made available from the corresponding author on reasonable request.

References

[1] Jeffrey C. Chandler, Sarah N. Bevins, Jeremy W. Ellis, Timothy J. Linder, Rachel M. Tell, Melinda Jenkins-Moore, J. Jeffrey Root, Julianna B. Lenoch, Suelee Robbe-Austerman, Thomas J. DeLiberto, Thomas Gidlewski, Torchetti Mia Kim, and Susan A. Shriner. SARS-CoV-2 exposure in wild white-tailed deer (*Odocoileus virginianus*). *Proceedings of the National Academy of Sciences*, 118(47): e2114828118, 2021. doi: 10.1073/pnas.2114828118.

[2] Vanessa L. Hale, Patricia M. Dennis, Dillon S. McBride, Jacqueline M. Nolting, Christopher Madden, Devra Huey, Margot Ehrlich, Jennifer Grieser, Jenessa Winston, Dusty Lombardi, Stormy Gibson, Linda Saif, Mary L. Killian, Kristina Lantz, Rachel M. Tell, Mia Torchetti, Suelee Robbe-Austerman,

Martha I. Nelson, Seth A. Faith, and Andrew S. Bowman. SARS-CoV-2 infection in free-ranging white-tailed deer. *Nature*, 602:481–486, 2022. doi: 10.1038/s41586-021-04353-x.

[3] Suresh V. Kuchipudi, Meera Surendran-Nair, Rachel M. Ruden, Michele Yon, Ruth H. Nissly, Kurt J. Vandegrift, Rahul K. Nelli, Lingling Li, Bhushan M. Jayarao, Costas D. Maranas, Nicole Levine, Katriina Willgert, Andrew J. K. Conlan, Randall J. Olsen, James J. Davis, James M. Musser, Peter J. Hudson, and Vivek Kapur. Multiple spillovers from humans and onward transmission of SARS-CoV-2 in white-tailed deer. *Proceedings of the National Academy of Sciences*, 119(6):e2121644119, 2022. doi: 10.1073/pnas.2121644119.

[4] Leonardo C. Caserta, Mathias Martins, Salman L. Butt, Nicholas A. Hollingshead, Lina M. Covaleda, Mia R. R. Everts, Krysten L. Schuler, and Diego G. Diel. White-tailed deer (*Odocoileus virginianus*) may serve as a wildlife reservoir for nearly extinct SARS-CoV-2 variants of concern. *Proceedings of the National Academy of Sciences*, 120, 2023. doi: 10.1073/pnas.2215067120.

[5] Aijing Feng, Sarah N. Bevins, Jeffrey C. Chandler, Thomas J. DeLiberto, Ria Ghai, Kristina Lantz, Julianna B. Lenoch, Adam Retchless, Susan A. Shriner, Cynthia Tang, Suxiang Sue Tong, Mia Torchetti, Anna Uehara, and Xiu-Feng Wan. Transmission of SARS-CoV-2 in the wild white-tailed deer in the United States. Unpublished.

[6] Kurt J. Vandegrift, Michele Yon, Meera Surendran Nair, Abhinay Gontu, Santhamani Ramasamy, Saranya Amirthalingam, Sabarinath Neerukonda, Ruth H. Nissly, Shubhada K. Chothe, Padmaja Jakka, Lindsey LaBella, Nicole Levine, Sophie Rodriguez, Chen Chen, Veda Sheersh Boorla, Tod Stuber, Jason R. Boulanger, Nathan Kotschwar, Sarah Grimké Aucoin, Richard Simon, Katrina L. Toal, Randall J. Olsen, James J. Davis, Dashzeveg Bold, Natasha N. Gaudreault, Krishani Dinali Perera, Yunjeong Kim, Chang Kyeong-Ok, Costas D. Maranas, Juergen A. Richt, James M. Musser, Peter J. Hudson, Vivek Kapur, and Suresh V. Kuchipudi. SARS-CoV-2 Omicron (B.1.1.529) infection of wild white-tailed deer in New York City. *Viruses*, 14:2770, 2022. doi: 10.3390/v14122770.

[7] Bradley Pickering, Oliver Lung, Finlay Maguire, Peter Kruczkiewicz, Jonathon D. Kotwa, Tore Buchanan, Marianne Gagnier, Jennifer L. Guthrie, Claire M. Jardine, Alex Marchand-Austin, Ariane Massé, Heather McClinchey, Kuganya Nirmalarajah, Patryk Aftanas, Juliette Blais-Savoie, Hsien-Yao Chee, Emily Chien, Winfield Yim, Andra Banete, Bryan D. Griffin, Lily Yip, Melissa Goolia, Matthew Suderman, Mahtieu Pinette, Greg Smith, Daniel Sullivan, Josip Rudar, Oksana Vernygora, Elizabeth Adey, Michelle Nebroski, Guillaume Goyette, Andrés Finzi, Geneviève Laroche, Ardeshir Ariana, Brett Vahkal, Marceline Côte, Allison J. McGeer, Larissa Nituch, Samira Mubareka, and Jeff Bowman. Di-

vergent SARS-CoV-2 variant emerges in white-tailed deer with deer-to-human transmission. *Nature Microbiology*, 7, 2022. doi: 10.1038/s41564-022-01268-9.

[8] Lukasz Rabalski, Maciej Kosinski, Natalia Mazur-Panasiuk, Boguslaw Szewczyk, Krystyna Bienkowska-Szewczyk, Ravi Kant, Tarja Sironen, Krzysztof Pyrc, and Maciej Grzybek. Zoonotic spill-over of SARS-CoV-2: mink-adapted virus in humans. *Clinical Microbiology and Infection*, 28(3):451.e1–451.e4, 2022. doi: 10.1016/j.cmi.2021.12.001.

[9] Bas B. Oude Munnink, Reina S. Sikkema, David F. Nieuwenhuijse, Robert Jan Molenaar, Emmanuelle Munger, Richard Molenkamp, Arco van der Spek, Paulien Tolsma, Ariene Rietveld, Miranda Brouwer, Noortje Bouwmeester-Vincken, Frank Harders, Renate Hakze-van den Honing, Marjolein C. A. Wegdam-Blans, Ruth J. Bouwstra, Corine GeurtsvanKessel, Annemiek van der Eijk, Francisca C. Velkers, Lidien A. M. Smit, Arjan Stegeman, Wim H. M. van der Poel, and Marion P. G. Koopmans. Transmission of SARS-CoV-2 on mink farms between humans and mink and back to humans. *Science*, 371(6525): 172–177, 2021.

[10] Gabriele Neumann, Takeshi Noda, and Yoshihiro Kawaoka. Emergence and pandemic potential of swine-origin H1N1 influenza virus. *Nature*, 459(7249):931–939, 2009. doi: 10.1038/nature08157.

[11] D. Vijaykrishna, L. L. M. Poon, H. C. Zhu, S. K. Ma, O. T. W. Li, C. L. Cheung, G. J. D. Smith, J. S. M. Peiris, and Y. Guan. Reassortment of pandemic H1N1/2009 influenza A virus in swine. *Science*, 328(5985):1529–1529, 2010. doi: 10.1126/science.1189132.

[12] CDC. Centers for Disease Control and Prevention update: Influenza A (H3N2)v transmission and guidelines — five states, 2011. *MMWR. Morbidity and mortality weekly report*, 60(51-52):1741–1744, 2012.

[13] Martha I. Nelson, Marie R. Gramer, Amy L. Vincent, and Edward C. Holmes. Global transmission of influenza viruses from humans to swine. *Journal of General Virology*, 93:2195–2203, 2012. doi: 10.1099/vir.0.044974-0.

[14] Mitchell V. Palmer, Mathias Martins, Shollie Falkenberg, Alexandra Buckley, Leonardo C. Caserta, Patrick K. Mitchell, Eric D. Cassmann, Alicia Rollins, Nancy C. Zylich, Randall W. Renshaw, Cassandra Guarino, Bettina Wagner, Kelly Lager, and Diego G. Diel. Susceptibility of white-tailed deer (*Odocoileus virginianus*) to SARS-CoV-2. *Journal of virology*, 95(11):e00083–21, 2021. doi: 10.1128/JVI.00083-21.

[15] Mathias Martins, Paola M. Boggiatto, Alexandra Buckley, Eric D. Cassmann, Shollie Falkenberg, Leonardo C. Caserta, Maureen H. V. Fernandes, Carly Kanipe, Kelly Lager, Mitchell V. Palmer,

and Diego G. Diel. From deer-to-deer: SARS-CoV-2 is efficiently transmitted and presents broad tissue tropism and replication sites in white-tailed deer. *PLoS pathogens*, 18(3):e1010197, 2022. doi: 10.1371/journal.ppat.1010197.

[16] Sarah A. Hamer, Chase Nunez, Christopher M. Roundy, Wendy Tang, Logan Thomas, Jack Richison, Jamie S. Benn, Lisa D. Auckland, Terry Hensley, Walter E. Cook, Alex Pauvolid-Corrêa, and Gabriel L. Hamer. Persistence of SARS-CoV-2 neutralizing antibodies longer than 13 months in naturally infected, captive white-tailed deer (*Odocoileus virginianus*), Texas. *Emerging microbes & infections*, 11(1):2112–2115, 2022. doi: 10.1080/22221751.2022.2112913.

[17] Sarah N. Bevins, Jeffrey C. Chandler, Scott Beckerman, David L. Bergman, Richard B. Chipman, Derek T. Collins, Joshua P. Eckery, Jeremy W. Ellis, Allen L. Gosser, Jonathon D. Heale, Jason Klemm, Kristina Lantz, Timothy J. Lindera, Robert Pleszewski, Christopher Quintanal, Jourdan Ringenberg, Kelsey R. Weir, Mia K. Torchetti, Juliana B. Lenoch, Thomas J. DeLiberto, and Susan A. Shriner. SARS-CoV-2 occurrence in white-tailed deer throughout their range in the continental United States. *bioRxiv*, 2023. doi: 10.1101/2023.04.14.533542. URL `https://www.biorxiv.org/content/10.1101/2023.04.14.533542v1`.

[18] Dillon S. McBride, Sofya K. Garushyants, John Franks, Steven H. Overend, Devra Huey, Amanda M. Williams, Seth A. Faith, Ahmed Kandeil, Sanja Trifkovic, Lance Miller, Trushar Jeevan, Anami Patel, Jaqueline M. Nolting, Michael J. Tonkovich, J. Tyler Genders, Andrew J. Montoney, Kevin Kasnyik, Timothy J. Linder, Sarah N. Bevins, Julianna B. Lenoch, Thomas J. DeLiberto, Eugene V. Koonin, Marc Suchard, Philippe Lemey, Richard J. Webby, Martha I. Nelson, and Andrew S. Bowman. Accelerated evolution of SARS-CoV-2 in free-ranging white-tailed deer. *Research Square*, rs.3.rs-2574993/v1, 2023. doi: 10.21203/rs.3.rs-2574993/v1. URL `https://www.researchsquare.com/article/rs-2574993/v1`.

[19] Steeve D. Côté, Thomas P. Rooney, Jean-Pierre Tremblay, Christian Dussault, and Donald M. Waller. Ecological impacts of deer overabundance. *Annual Review of Ecology, Evolution, and Systematics*, 35: 113–147, 2004. doi: 10.1146/annurev.ecolsys.35.021103.105725.

[20] James D. Nichols, Tiffany L. Bogich, Emily Howerton, Ottar N. Bjørnstad, Rebecca K. Borchering, Matthew Ferrari, Murali Haran, Christopher Jewell, Kim M. Pepin, William J. M. Probert, Juliet R. C. Pulliam, Michael C. Runge, Michael Tildesley, Cécile Viboud, and Katriona Shea. Strategic testing approaches for targeted disease monitoring can be used to inform pandemic decision-making. *PLoS biology*, 19(6):e3001307, 2021. doi: 10.1371/journal.pbio.3001307.

[21] Eamon B. O'Dea, Kim M. Pepin, Ben A. Lopman, and Claus O. Wilke. Fitting outbreak models to data from many small norovirus outbreaks. *Epidemics*, 6:18–29, 2014. doi: 10.1016/j.epidem.2013.12.002.

[22] Giovanni Lo Iacono, Andrew A. Cunningham, Elisabeth Fichet-Calvet, Robert F. Garry, Donald S. Grant, Melissa Leach, Lina M. Moses, Gordon Nichols, John S. Schieffelin, Jeffrey G. Shaffer, Colleen T. Webb, and James L. N. Wood. A unified framework for the infection dynamics of zoonotic spillover and spread. *PLoS neglected tropical diseases*, 10(9):e0004957, 2016. doi: 10.1371/journal.pntd.0004957.

[23] Sebastian Meyer and Leonhard Held. Incorporating social contact data in spatio-temporal models for infectious disease spread. *Biostatistics*, 18(2):338–351, 2017. doi: 10.1093/biostatistics/kxw051.

[24] Kathleen A. Alexander, Colin J. Carlson, Bryan L. Lewis, Wayne M. Getz, Madhav V. Marathe, Stephen G. Eubank, Claire E. Sanderson, and Jason K. Blackburn. The ecology of pathogen spillover and disease emergence at the human-wildlife-environment interface. In Christon J. Hurst, editor, *The connections between ecology and infectious disease*, pages 267–298. Springer International Publishing, 2018. ISBN 978-3-319-92373-4. doi: 10.1007/978-3-319-92373-4_8.

[25] Christina L. Faust, Hamish I. McCallum, Laura S. P. Bloomfield, Nicole L. Gottdenker, Thomas R. Gillespie, Colin J. Torney, Andrew P. Dobson, and Raina K. Plowright. Pathogen spillover during land conversion. *Ecology letters*, 21:471–483, 2018. doi: 10.1111/ele.12904.

[26] Hyokyoung G. Hong and Yi Li. Estimation of time-varying reproduction numbers underlying epidemiological processes: A new statistical tool for the COVID-19 pandemic. *PloS ONE*, 15(7):e0236464, 2020. doi: 10.1371/journal.pone.0236464.

[27] Mark Q. Wilber, Colleen T. Webb, Fred L. Cunningham, Kerri Pedersen, Xiu-Feng Wan, and Kim M. Pepin. Inferring seasonal infection risk at population and regional scales from serology samples. *Ecology*, 101(1):e02882, 2020.

[28] Aadrita Nandi and Linda J.S. Allen. Probability of a zoonotic spillover with seasonal variation. *Infectious Disease Modelling*, 6:514–531, 2021. doi: 10.1016/j.idm.2021.01.013.

[29] USGS. U.S. Geological Survey Gap Analysis Project (GAP), White-tailed Deer (*Odocoileus virginianus*) mWTDEx_CONUS_2001v1 Habitat Map: U.S. Geological Survey data release. 2018. doi: 10.5066/F7SF2TM0.

[30] Kim M. Pepin, Amy J. Davis, Daniel G. Streicker, Justin W. Fischer, Kurt C. VerCauteren, and Amy T. Gilbert. Predicting spatial spread of rabies in skunk populations using surveillance data reported by the public. *PLoS Neglected Tropical Diseases*, 11(7):e0005822, 2017. doi: 10.1371/journal.pntd.0005822.

[31] Daniel J. O'Brien, Stephen M. Schmitt, Jean S. Fierke, Stephanie A. Hogle, Scott R. Winterstein, Thomas M. Cooley, William E. Moritz, Kelly L. Diegel, Scott D. Fitzgerald, Dale E. Berry, and John B. Kaneene. Epidemiology of *Mycobacterium bovis* in free-ranging white-tailed deer, Michigan, USA, 1995–2000. *Preventive Veterinary Medicine*, 54:47–63, 2002. doi: 10.1016/S0167-5877(02)00010-7.

[32] Michael W. Miller and Mary M. Conner. Epidemiology of chronic wasting disease in free-ranging mule deer: spatial, temporal, and demographic influences on observed prevalence patterns. *Journal of Wildlife Diseases*, 41(2):275–290, 2005. doi: 10.7589/0090-3558-41.2.275.

[33] Daniel A. Grear, Michael D. Samuel, Julie A. Langenberg, and Delwyn Keane. Demographic patterns and harvest vulnerability of chronic wasting disease infected white-tailed deer in Wisconsin. *The Journal of Wildlife Management*, 70(2):546–553, 2006. doi: 10.2193/0022-541X(2006)70[546:DPAHVO]2.0.CO;2.

[34] Charles A. DeYoung. Population dynamics. In David G. Hewitt, editor, *Biology and management of white-tailed deer*, pages 160–193. CRC Press, 2011. ISBN 9780429078750. doi: 10.1201/9781482295986.

[35] Daniel J. Storm, Michael D. Samuel, Robert E. Rolley, Paul Shelton, Nicholas S. Keuler, Bryan J. Richards, and Timothy R. Van Deelen. Deer density and disease prevalence influence transmission of chronic wasting disease in white-tailed deer. *Ecosphere*, 4(1):1–14, 2013. doi: 10.1890/ES12-00141.1.

[36] U.S. Census Bureau. County population totals: 2020–2021. U.S. Department of Commerce. https://data.census.gov/data/tables/time-series/demo/popest/2020s-counties-total.html. 2020.

[37] Sudipto Banerjee, Bradley P. Carlin, and Alan E. Gelfand. *Hierarchical modeling and analysis for spatial data*. Chapman and Hall/CRC, Boca Raton, FL, second edition, 2015. ISBN 9781439819173.

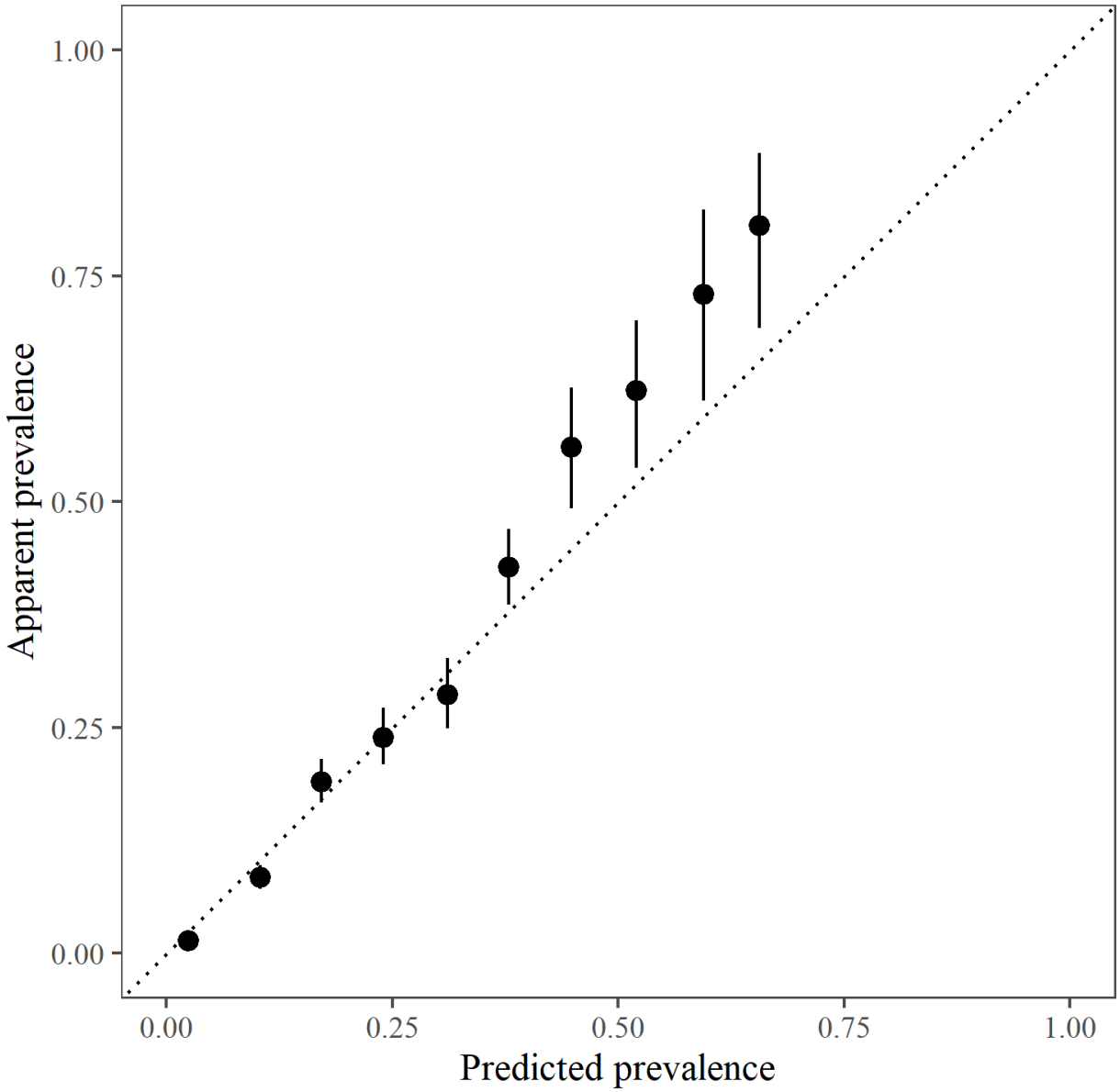

Figure 1: Calibration curve, comparing in-sample predictions of infection risk p_k (i.e., predicted prevalence) to observed outcomes against a 1:1 reference line (dotted line). Apparent prevalence (proportion of positive test results per group) is computed for model-fit diagnostic groups formed by binning predicted prevalence into 10 ranges. Error bars depict standard, frequentist 95% confidence intervals for each apparent prevalence group.

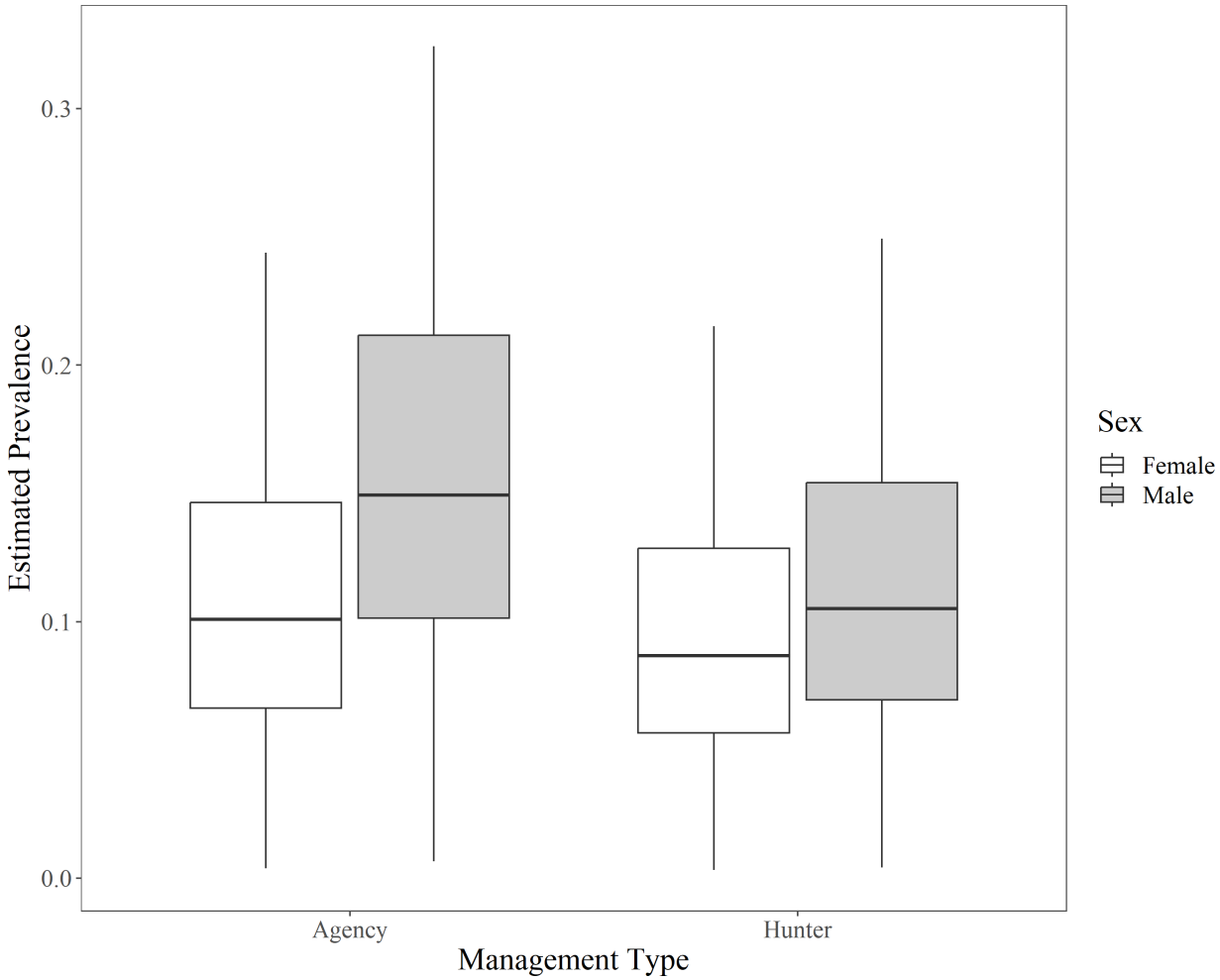

Figure 2: Distributions of posterior estimates for time-averaged prevalence across counties from October 2021 through March 2022 for different demographic groups and management types.

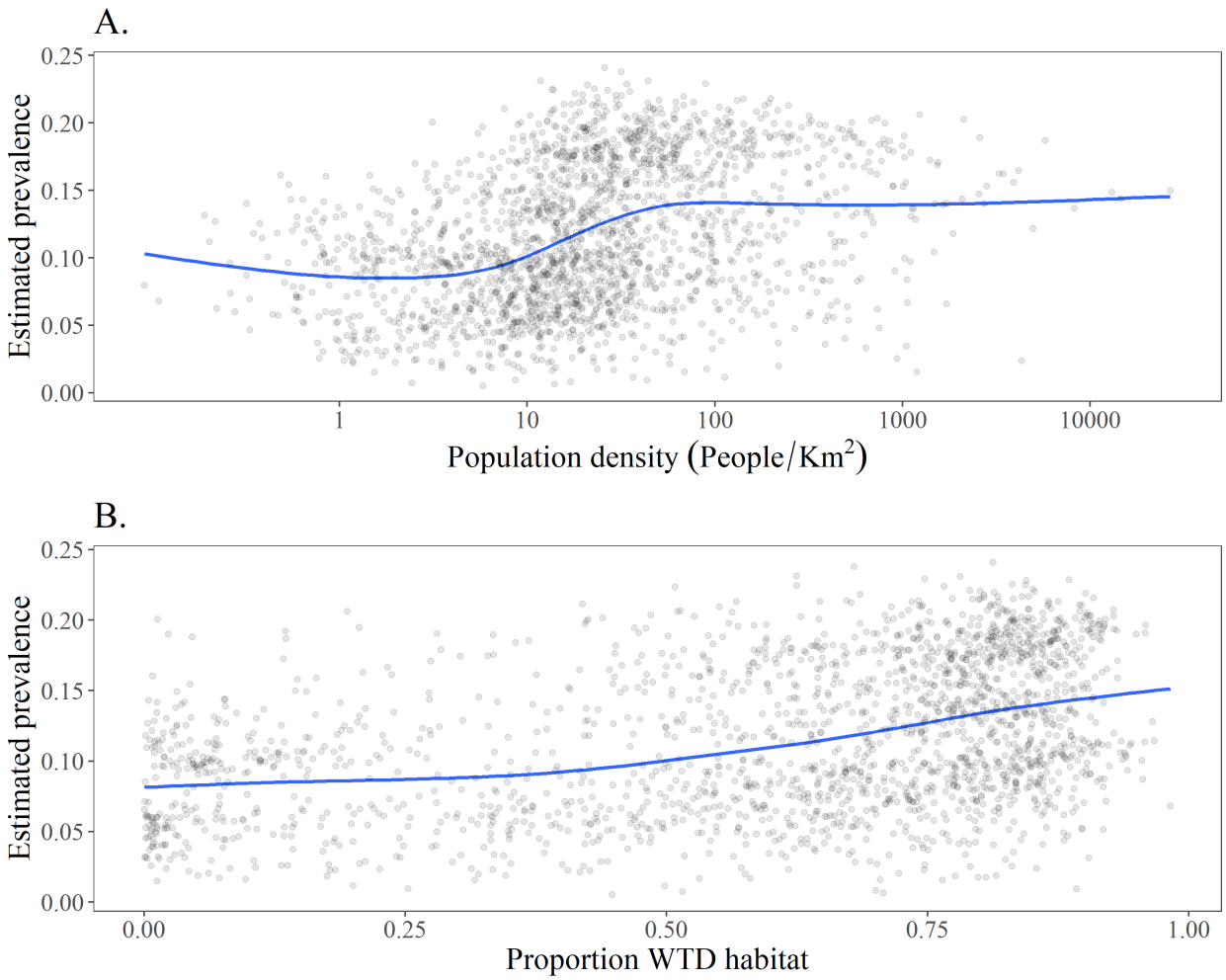

Figure 3: Estimates for time-averaged prevalence across counties plotted against ecological covariates from October 2021 through March 2022, with empirical trend line overlaid (blue; GAM smoother). Each point in the plot represents the time-averaged prevalence for one county.

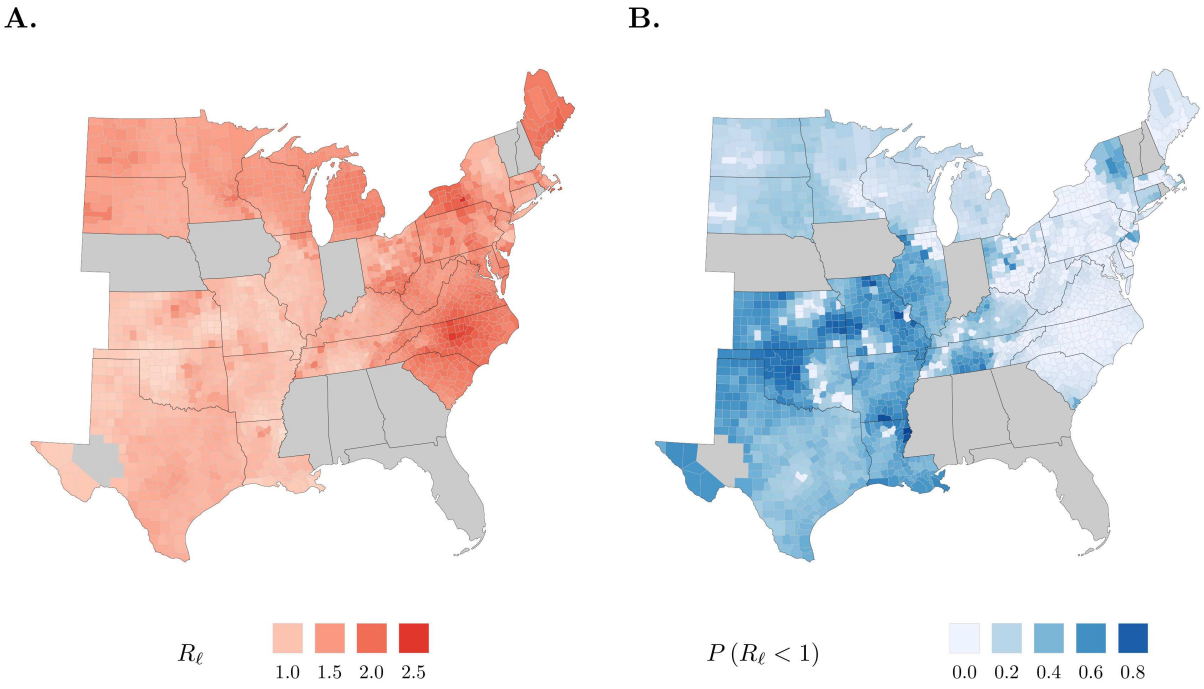

Figure 4: A) Estimates for local epidemiological reproduction number R_ℓ and B) uncertainty (posterior probability that $R_\ell < 1$). States that did not participate in the study are greyed out. Counties estimated through the GAP WTD species distribution model to not support WTD populations are also greyed out.

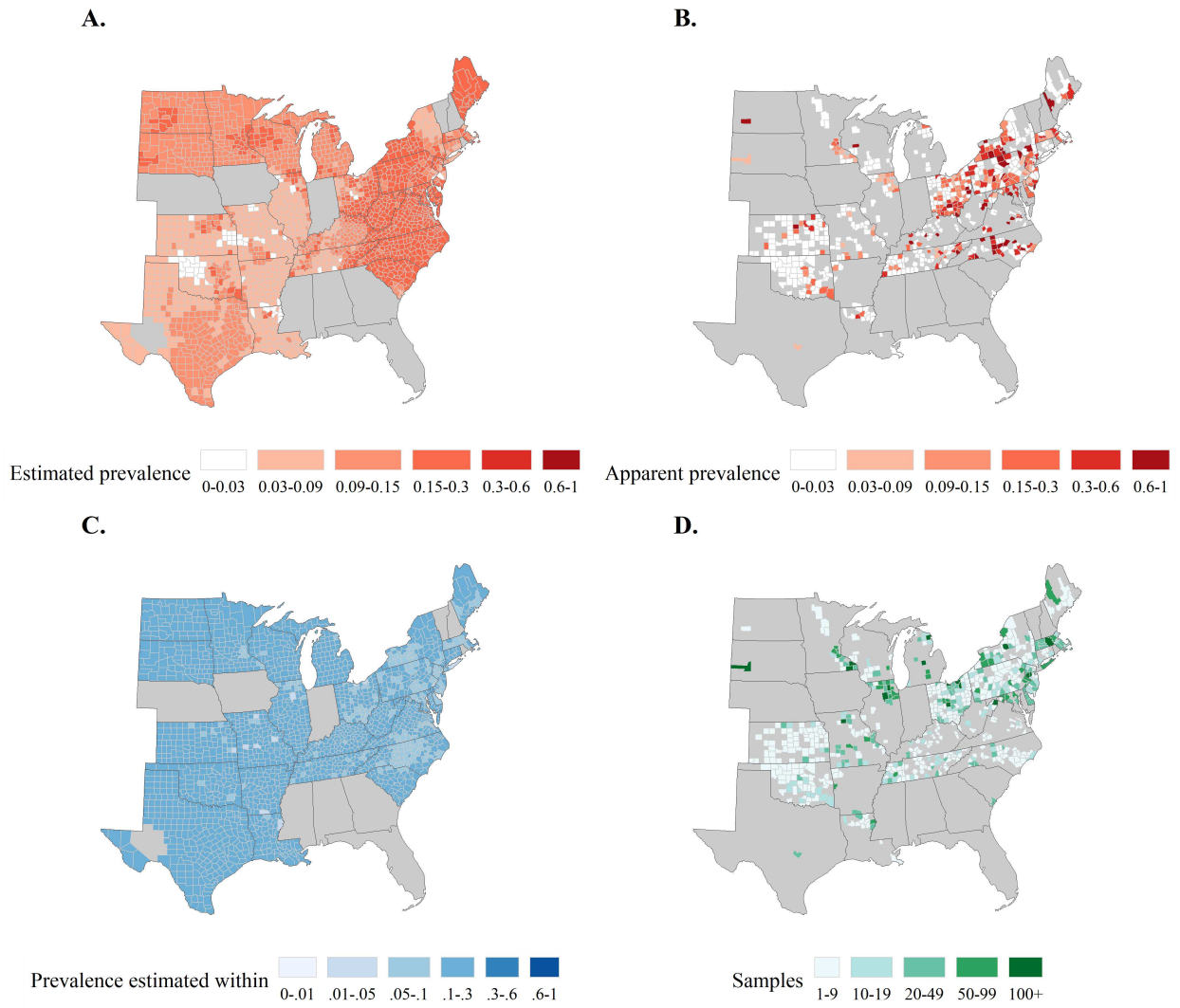

Figure 5: A) Estimates for time-averaged prevalence from October 2021 through March 2022, B) apparent prevalence from October 2021 through March 2022, C) uncertainty for estimated prevalence (maximum half-width of 95% highest posterior density interval), and D) number of samples collected from each county. Grey shading is as described for Figure 4.

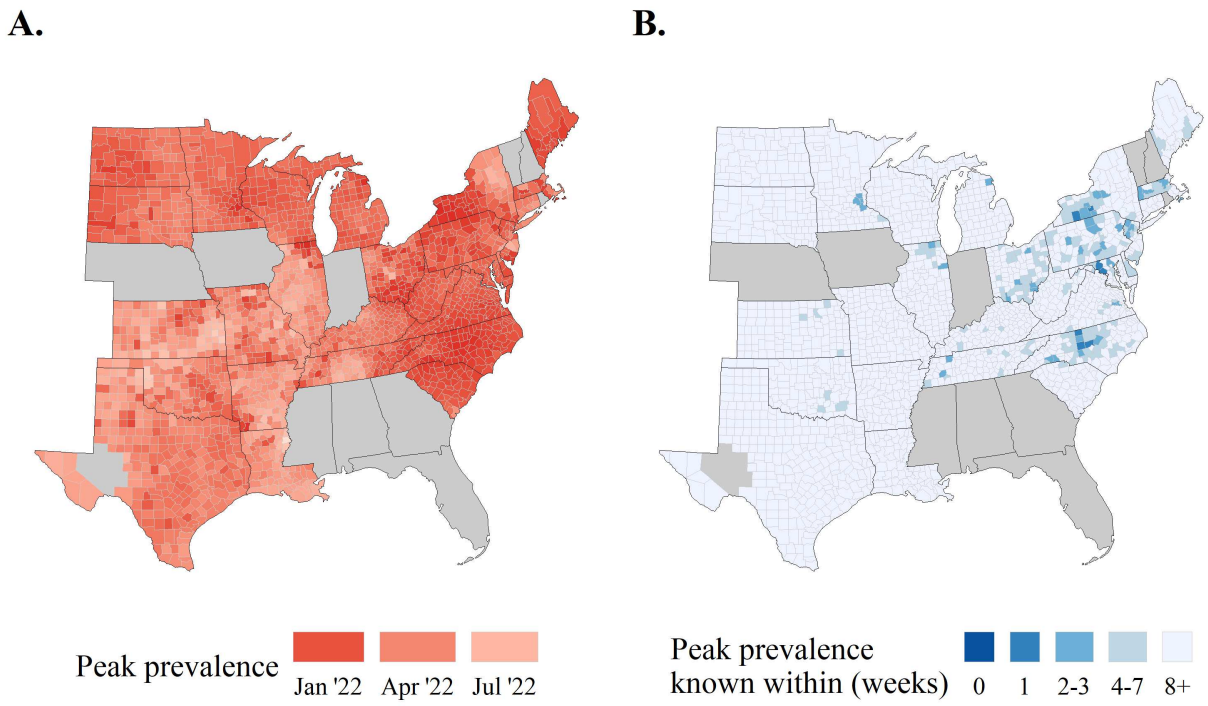

Figure 6: A) Estimates for peak prevalence time with B) uncertainty (maximum half-width of 95% highest posterior density interval). Grey shading is as described for Figure 4.

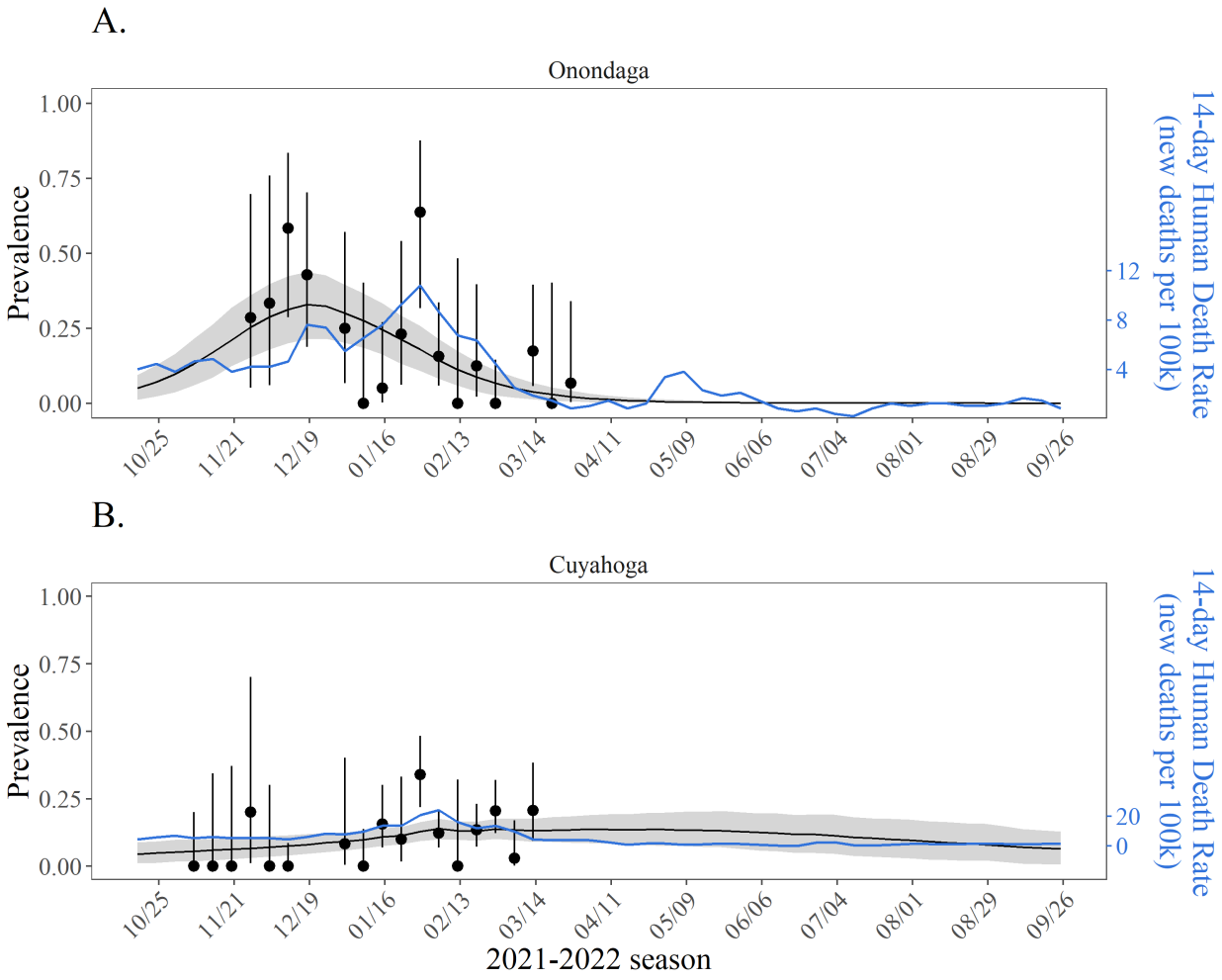

Figure 7: Estimated prevalence with uncertainty (maximum half-width of 95% highest posterior density interval) in the two most intensively sampled counties, A) Onondaga County, New York (252 samples), and B) Cuyahoga County, Ohio (609 samples). Blue time series shows the human death rate for both counties during the same time period.

Table 1: Parameter descriptions and posterior distribution summaries for regression effects and spatial parameters. Posterior distribution summaries include the posterior mean, 95% highest posterior density interval (HPDI), and posterior standard deviation (s.d.).

Component	Parameter	Covariate	Type	Post. mean	95% HPDI	Post. s.d.
p_k	a_1	$z_{k1} = 1$	Intercept	1.95	(1.17, 2.69)	0.39
	a_2	$z_{k2} = (\text{Male})_k$	Group indicator	0.59	(0.35, 0.85)	0.13
	a_3	$z_{k3} = (\text{Juvenile})_k$	Group indicator	0.17	(−0.06, 0.41)	0.12
	a_4	$z_{k4} = (\text{Hunter harvest})_k$	Group indicator	−0.17	(−0.56, 0.22)	0.20
	a_5	$z_{k5} = (\text{Other management})_k$	Group indicator	−0.13	(−0.57, 0.34)	0.23
	a_6	$z_{k6} = (\text{Oral swab})_k$	Sample indicator	0.28	(−0.41, 0.98)	0.36
	a_7	$z_{k7} = (\text{Unknown swab})_k$	Sample indicator	1.50	(0.67, 2.40)	0.45
	a_8	$z_{k8} = (\text{Human death rate})_k$	Spillover pressure proxy	0.14	(0.00, 0.29)	0.07
	a_9	$z_{k9} = z_{k2}z_{k3}$	Interaction (Sex/Age)	−0.29	(−0.60, 0.05)	0.17
	a_{10}	$z_{k10} = z_{k2}z_{k4}$	Interaction (Sex/Management)	−0.32	(−0.61, −0.01)	0.15
	a_{11}	$z_{k11} = z_{k2}z_{k5}$	Interaction (Sex/Management)	−0.34	(−0.81, 0.16)	0.25
	a_{12}	$z_{k12} = z_{k4}z_{k6}$	Interaction (Management/Col'n.)	−0.05	(−0.87, 0.80)	0.43
	a_{13}	$z_{k13} = z_{k5}z_{k6}$	Interaction (Management/Col'n.)	−0.25	(−1.63, 1.15)	0.71
	a_{14}	$z_{k14} = z_{k4}z_{k7}$	Interaction (Management/Col'n.)	0.44	(−2.25, 3.42)	1.46
R_ℓ	b_1	$x_{\ell 1} = 1$	Intercept	−3.76	(−4.10, −3.32)	0.20
	b_2	$x_{\ell 2} = \log(\text{Human pop. density})_\ell$	County data	0.06	(−0.02, 0.16)	0.05
	b_3	$x_{\ell 3} = (\text{Prop. WTD habitat})_\ell$	County data	0.10	(−0.01, 0.24)	0.06
η_ℓ	τ_ℓ	N/A	Spatial precision	2.23	(0.51, 4.54)	1.12
	γ_ℓ	N/A	Spatial range	1.00	(0.99, 1.00)	0.00
$t_{0,\ell}$	τ_{t_0}	N/A	Temporal precision	0.07	(0.04, 0.12)	0.02
	γ_{t_0}	N/A	Temporal range	1.00	(0.99, 1.00)	0.00
$r_\ell(t)$	γ	N/A	Recovery rate	0.86	(0.53, 1.18)	0.17

Supplementary Files

This is a list of supplementary files associated with this preprint. Click to download.

- supplement.pdf